Journal of Structural Geology, Vol. 15, Nos 3–5, pp. 265 to 276, 1993
Printed in Great Britain

0191-8141/93 $06.00+0.00

Crystallographic preferred orientation development in a buckled single layer: a computer simulation

Y. ZHANG

Department of Earth Sciences, Monash University, Clayton, Victoria 3168, Australia

B. E. HOBBS

CSIRO Division of Geomechanics, P.O. Box 54, Mt. Waverley, Victoria 3149, Australia

and

M. W. JESSELL

Department of Earth Sciences, Monash University, Clayton, Victoria 3168, Australia

(*Received* 16 *December* 1991; *accepted in revised form* 1 *August* 1992)

Abstract—The development of crystallographic preferred orientation in a single-layer buckling assembly has been numerically simulated using an explicit, finite difference computer code, FLAC. The model treats the materials in the single competent layer and the embedding less competent matrix as a polycrystalline aggregate with one slip system, which exhibits elastic–perfectly-plastic behaviour, and assumes dislocation glide as the dominant strain accommodation mechanism. The results show that the preferred orientation of slip planes is much better developed in the less competent matrix than in the buckled competent layer. This correlates with the low strains developed in the layer and the high strains in the matrix. The competency contrast in the model also influences the fabric development, since changing the contrast effectively alters the final buckle size and strain distributions. The patterns of the preferred orientations vary throughout the assembly, showing different orientation relationships to the fold axial plane. The slip planes are generally preferably oriented approximately parallel to the local principal extension direction.

INTRODUCTION

SINGLE-LAYER buckling has been extensively studied since the 1950s. The main outcome of these studies has been the dominant wavelength and wavelength selection theories which were first proposed by Biot (1957, 1959a,b, 1961) and Ramberg (1959, 1960, 1961), and were then modified by other investigators (e.g. Chapple 1968, Sherwin & Chapple 1968, Hudleston 1973a,b). Contrasting with these widely quoted theories are the results of Cobbold (1975, 1977), demonstrating the propagating evolution of folds, and Williams *et al.* (1978) and Abbassi & Mancktelow (1990), emphasizing the effects of initial perturbation geometries.

It is noted that previous simulations of fold development concentrated on the buckling geometry of a single competent layer, whereas the internal fabric development associated with the buckled layer was often ignored. We are focusing on this aspect since the grain scale fabric is often a major structural element in the field investigation of natural folds. In the present study we have modelled the development of crystallographic preferred orientation in a buckled single layer and the embedding matrix, both consisting of polycrystalline grains with one slip system, employing the computer code FLAC (Fast Lagrangian Analysis of Continua, Cundall & Board 1988).

The choice of a single slip system material may be a weakness of the model. However, this specification achieves a unique orientation relationship between slip planes and principal deformation axes, which makes it possible to correlate the alignment of slip planes with cleavage development. Besides, some crystals do show the domination of one slip system (e.g. olivine, ice and quartz deformed under low temperature) (see Nakaya 1954, Nicolas & Poirier 1976).

MODEL DESCRIPTION

FLAC is an explicit, time-marching computer code which combines three important aspects: the finite difference method; the law of motion; and the stress–strain constitutive equations of several mechanical models (Cundall & Board 1988). The code simulates geological materials in terms of a mesh comprising quadrilateral elements subdivided into four overlaid constant strain triangles; the deformation of each element follows the prescribed stress–strain law according to the applied boundary conditions (e.g. a bulk strain increment). It should be pointed out that the element matrices of FLAC are identical to those of the finite element method for constant-strain triangles, although they are formed by the finite difference method.

A large number of validation tests of FLAC have been carried out in the mining and civil engineering fields

(Cundall & Board 1988, Itasca Consulting Group 1991). The FLAC results generally are in good agreement with those calculated by analytical methods. In particular, the results show that FLAC is capable of modelling the deformation across a material boundary surface or an interface. Furthermore, FLAC has also been used for the studies of graben faulting (Cundall 1990) and shear band–strain localization (Cundall 1989, Hobbs & Ord 1989, Hobbs *et al.* 1990, Ord 1990).

For the current purpose, the 'ubiquitous joint model' (a constitutive model in FLAC) was chosen. This model treats each crystal grain of an aggregate as an elastic–perfectly-plastic material containing an infinite number of parallel slip planes (one slip system); the slip planes also follow elastic–perfectly-plastic behaviour, and their orientations can be arbitrarily initialized for different grains in the polycrystals. In such a material, the total strain increment ($\Delta\varepsilon$) is assumed to be composed of an elastic part ($\Delta\varepsilon^e$) and a plastic part ($\Delta\varepsilon^p$), that is,

$$\Delta\varepsilon = \Delta\varepsilon^e + \Delta\varepsilon^p, \tag{1}$$

where $\Delta\varepsilon^e$, achieved before plastic yielding, is defined by Hooke's law, and $\Delta\varepsilon^p$, achieved after plastic yielding, is defined by the non-associated flow law (see Board 1989 for the full description of the constitutive equations). Plastic yielding can occur on the slip planes, or in the medium material in which the slip planes are embedded, or both. This is determined by the values of slip plane and medium material cohesions, and slip plane orientations. Slip (plastic yielding) on a slip plane commences when the resolved shear stress (τ_r) on the slip plane is equal to the critical resolved shear stress (τ_c); τ_c is determined by the value of slip plane cohesion (C_s) after zero slip-plane friction is chosen. Similarly, when the maximum shear stress (τ_m) in the medium materials reaches the yielding limit (σ_o), plastic flow in the medium materials will start; σ_o is correspondingly determined by medium material cohesion (C_m) after the internal friction angle is set to be zero. These indicate that the following conditions must be satisfied:

$$\begin{aligned} \tau_r &\leq \tau_c \\ \tau_m &\leq \sigma_o. \end{aligned} \tag{2}$$

The slip and the medium deformation produce distinct incremental strains. The former leads to material shifting along slip planes, while the latter causes the distortion of the material between two slip planes. In practice, the second deformation effect can be viewed as being equivalent to that caused by climb and vacancy diffusion. By setting $C_m > C_s$ so that $\sigma_o > \tau_c$, slip (dislocation glide) will be easier than plastic flow in the medium, and slip will dominate and accommodate the major part of the plastic deformation. The plastic flow in the medium material plays only a supplementary role. The imposed bulk strain is therefore compatibly accommodated by the co-operation of two mechanisms.

The polycrystalline deformation model described above differs from the Taylor–Bishop–Hill model (Lister *et al.* 1978) in four main ways: (1) only one slip system is involved; (2) slip planes can experience some small elastic deformation before slip; (3) there is a medium material between slip planes which is allowed to deform; and (4) the homogeneous strain assumption is abandoned while strain compatibility is still maintained, and strain as well as stress distributions are instead determined by solving a set of constitutive equations.

NUMERICAL SPECIMEN SPECIFICATION

The finite difference mesh (Fig. 1) chosen for these simulations is 100 × 60 in size, and the central 16 rows of elements are used for the single competent layer surrounded by the less competent matrix. The competent layer, with a length/thickness ratio of 20:1, possesses a small symmetric perturbation. As shown in Fig. 2, slip planes have been randomly assigned to each element in the competent layer and in the areas of the matrix adjoining the layer, where each element can be thought of as corresponding to a crystal grain with a single slip system. The slip-plane traces and the the orientation distribution of slip-plane normals show that the distributions of slip planes are initially random and uniform both in the layer and the matrix. The areas of the matrix that are relatively remote from the layer are not initialized with slip planes, simply because they are less interesting in terms of fabric investigation as they display a relatively homogeneous strain response. Instead, they simply act as an isotropic and homogeneous elastic–perfectly-plastic material. The purpose of this specification is to save computer time.

The material properties then have to be assigned to the numerical specimen assembly. For single-layer buckle folding, an important parameter is the competency contrast (R) between the competent layer and the less competent matrix. The elastic–perfectly-plastic behaviour of the currently chosen material means that the competency contrast is dominantly determined by the ratio of cohesion between the layer and the matrix; the cohesions determine when the material commences plastic deformation and how much stresses the material can sustain. However, since the material incorporates some elastic behaviour, the elastic constants are also taken into consideration in defining the contrast. The definition of R therefore is:

$$R = \frac{C_s}{C_s^o} = \frac{C_m}{C_{m1}^o} = \frac{C_s}{C_{m2}^o} = \frac{K}{K^o} = \frac{G}{G^o}, \tag{3}$$

where C_s, C_m and C_s^o, C_{m1}^o are the slip plane and material cohesions for the competent layer and the less competent matrix with slip-plane involvement, respectively, C_{m2}^o is the material cohesion for the less competent matrix without slip plane involvement, and K, G and K^o, G^o are the bulk and shear moduli for the layer and the matrix, respectively. The values of R = 5 and 100 are adopted for the two numerical experiments described here. To achieve this C_s, C_m, K and G are chosen as 2×10^9, 2×10^{10}, 4.64×10^{10} and 4.23×10^{10} Pa,

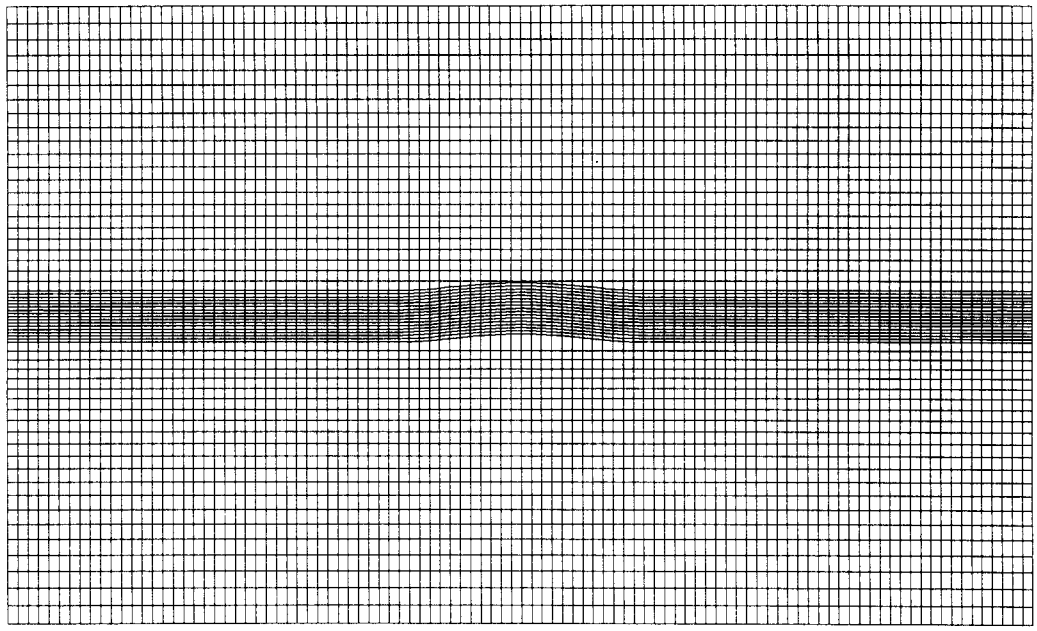

Fig. 1. The initial finite difference mesh used in the simulation. The competent layer occupies the central 16 rows of elements.

respectively, and the properties for the less competent matrix (C_s^o, C_{m1}^o, C_{m2}^o, K^o,G^o) are correspondingly determined according to equation (3) and the required R values. A density of 2650 kg m^{-3} and zero friction are used for both the layer and the matrix. It must be clarified that, except for the values of density, K and G, which are chosen with reference to those for quartzites (Clark 1966), the other parameters are used simply out of the need to construct the model.

The numerical specimen is then subjected to a pure shearing deformation, with shortening parallel to the layer at a rate of 1×10^{-3} units per time step; the unit is the initial length of an element in the horizontal direction (see Fig. 1). A 20% overall shortening of the specimen requires 20,000 steps of computation, which takes 7 days on a 386sx computer.

FABRIC DEVELOPMENT

After 20% overall shortening, well-shaped buckles have developed in competent layers (Fig. 3). Consistent

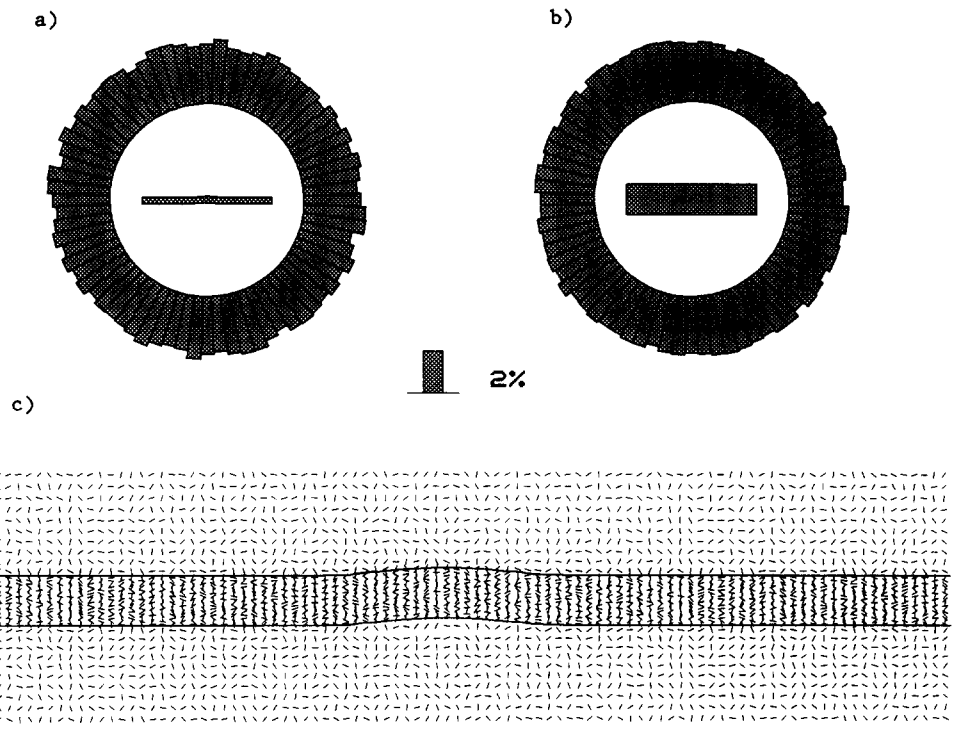

Fig. 2. (a) & (b) The initial orientation distributions of the slip-plane normals with respect to the specimen orientation for the competent layer and the matrix, respectively. (c) The initial slip-plane traces in the specimen.

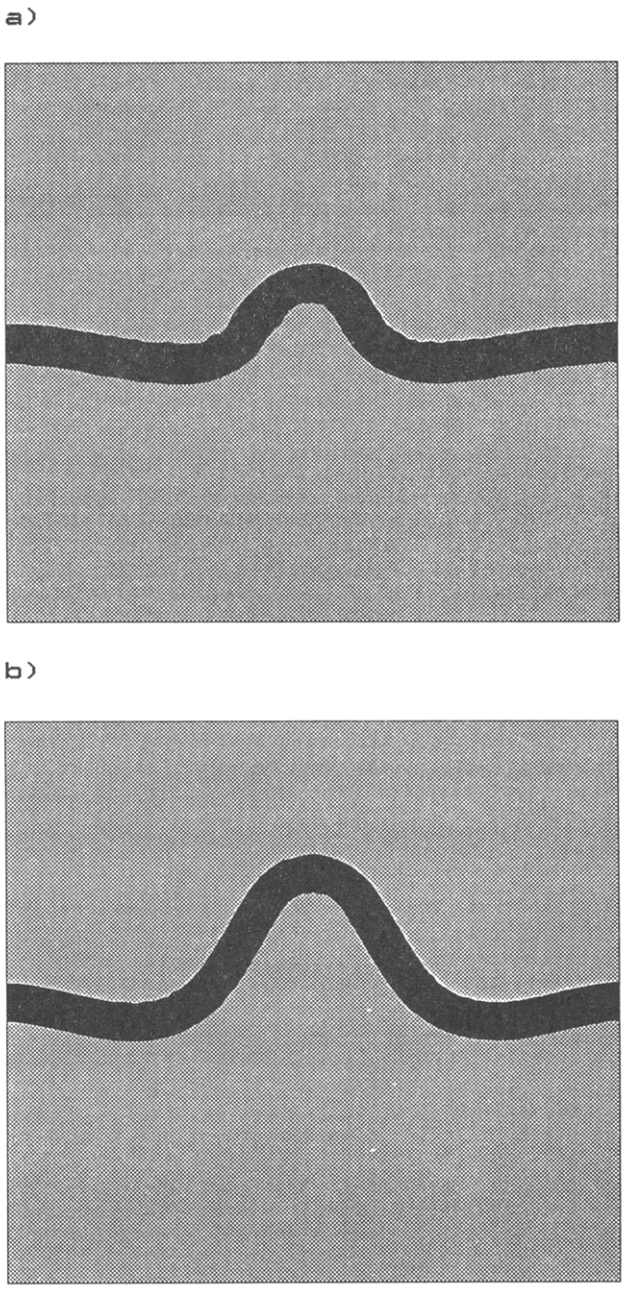

Fig. 3. The final geometries of the buckled layers after 20% overall shortening: (a) the model of R =5; (b) the model of R = 100.

with the dependence of fold wavelength on the competency contrast, which is predicted by the Biot–Ramberg theory, the fold developed in the deformed numerical specimen with R = 5 exhibits smaller wavelength and amplitude than that for the fold under a specification of R = 100. Separate fabric analyses of slip planes have been performed for the buckled layer and the shortened matrix.

Competent layer

The final slip-plane traces in the buckled layers and the corresponding orientation distribution of the slip-plane normals are illustrated in Fig. 4. Comparison with the starting configuration (Fig. 2) shows that the slip planes have been systematically rotated accompanying the buckling and also some shortening of the competent layers, and the local rotations in the buckled parts of the layers are dominated by the spin induced by buckling. However, the orientation distribution of the total slip-plane normals in each competent layer for two models (Fig. 4b) still display an approximately uniform pattern, even though the results for the model with R = 5 exhibit a slight concentration of the slip-plane normals parallel to the overall shortening direction. This indicates that, after 20% overall shortening and significant buckling, no evident preferred orientation of slip planes is developed in the competent layers as a whole.

The fold geometry could cause possible mixing effects in the fabric presentation. For example, the fabric patterns in the outer arc and inner arc areas of a fold hinge zone could neutralize each other. To investigate this effect, detailed fabric analysis was conducted for different parts of the fold. On the basis of the similar finite strain geometries, the buckled competent layers are divided into five sub-areas (Figs. 5 and 6). They are the left and right limb areas (1 and 2), the outer and inner arc areas (3 and 4) of the hinge zone, and the unbuckled layer area (5). The orientation distributions of the slip-plane normals in these subareas for the two models (see Fig. 5 for R = 5 and Fig. 6 for R = 100) show clear variation.

(1) *The limb areas*: for the model with R = 5, the maxima of slip-plane normals for the two limbs are both oblique to the fold axial plane but approximately parallel to the respective limb layer plane, indicating that the most prevalent alignment of slip planes occurred normal to the limb layer planes. In contrast, the orientation distribution of slip plane normals for the model with R = 100 is still approximately uniform, not displaying any preferred orientations.

(2) *The outer arc area*: an evident maximum of slip-plane normals develops parallel to the fold axial plane for the model with R = 5, whereas for the model with R = 100, only a slightly higher concentration is observed about the orientation of the axial plane.

(3) *The inner arc area*: the concentration of slip-plane normals for the model of R = 5 is stronger than for the model of R = 100. The orientation of the maximum concentration is opposite to that for the outer arc area, roughly normal to the axial plane.

(4) *The unbuckled layer area*: the distribution of slip-plane normals shows a maximum parallel to the bulk shortening direction for the model of R = 5, but no evident preferred orientation is observed for the model of R = 100.

In summary, the competent layers of the two models show different patterns of fabric development. The high competency contrast model (R = 100) is associated with a very poor fabric development. In contrast, the fabric development in the low competency contrast model (R = 5) is stronger. This behaviour is dependent on the mechanical behaviour and deformation feature of a competent layer, both of which will vary for different layer-matrix assemblies with different competency contrasts. More discussion will be given later.

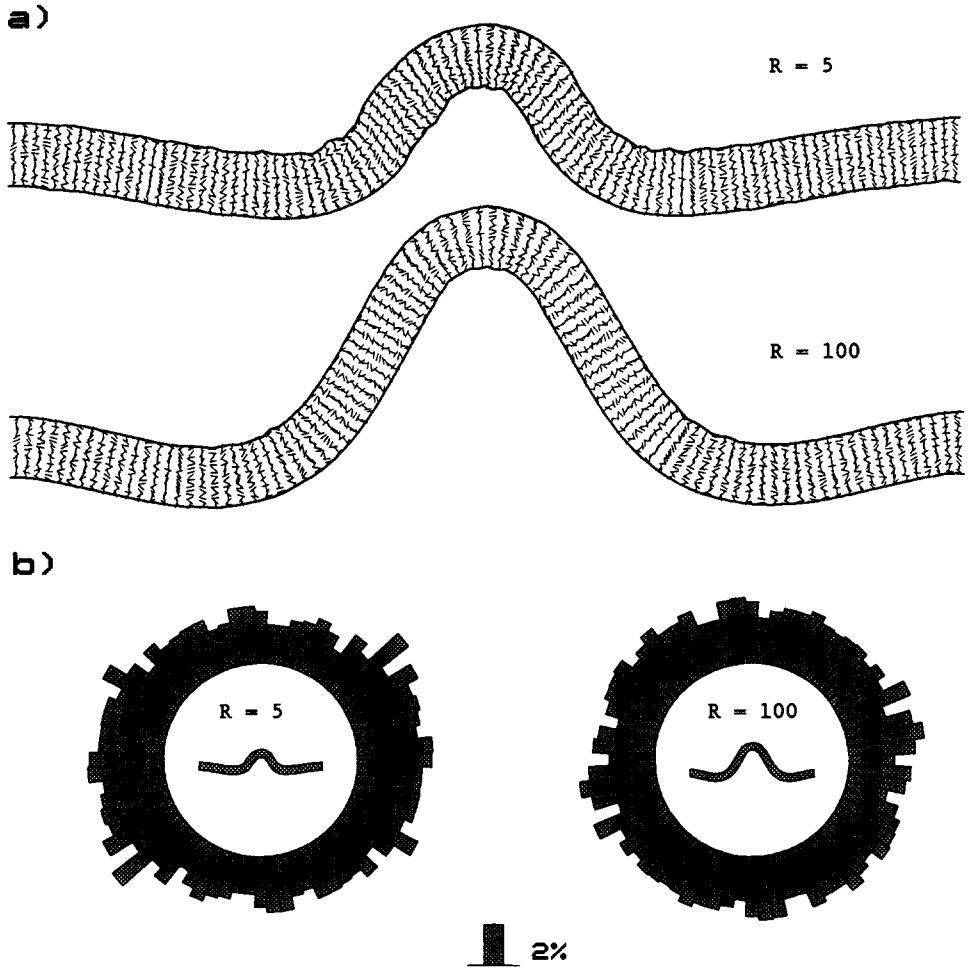

Fig. 4. (a) The spatial distribution of slip-plane traces in the buckled competent layers. (b) The corresponding orientation distribution patterns of slip-plane normals with respect to the specimen orientations for the whole layer in the two models.

Less competent matrix

The final distributions of slip-plane traces in the shortened matrix for the two models with $R = 5$ and 100 are presented in Figs. 7(a) and 8(a), respectively. As within the buckled layer, it can be seen that the patterns of slip-plane alignment correlate with position with respect to the buckled competent layers. Based on the styles of slip-plane alignments, six sub-areas can be defined from each matrix of the two models, both numbered from 1 to 6 (Figs. 7a and 8a). The corresponding orientation distributions of slip-plane normals for these sub-areas are given in Figs. 7(b) and 8(b), respectively, for the model with $R = 5$ and the model with $R = 100$. It is evident from these figures that the preferred orientations are well developed. The main fabric features for the different areas are summarized as follows.

(1) *Area* 1 (*outer arc of the fold hinge zone*): for the model with $R = 100$, the preferred orientation of slip-plane normals is a maximum parallel to the fold axial plane, indicating a prevalent alignment of slip planes normal to the fold axial plane. For the model of $R = 5$, however, no evident preferred orientation is developed.

(2) *Area* 2 (*inner arc of the fold hinge zone*): the two models show similar fabrics, that is, a single maximum of slip-plane normals normal to the fold axial plane. The intensity of the maximum of the model with $R = 100$ is stronger.

(3) *Areas* 3 *and* 4 (*outer arcs of the fold limbs*): for both models, the preferred orientations of slip-plane normals for the two areas are oblique to, but symmetric about, the fold axial plane. The maximum for each of the areas is roughly parallel to the corresponding limb. It is noted that the two areas with the above fabric features in the model of $R = 5$ have shrunk relative to those in the model of $R = 100$.

(4) *Areas* 5 *and* 6 (*inner arcs of the fold limbs*): the respective preferred orientations of slip-plane normals for the two areas are again roughly symmetrically oblique to the fold axial plane. Contrary to the results for areas 3 and 4, however, the two maxima are inclined in the opposite direction to that of the respective relevant limb. The difference between the two models is that the model of $R = 5$ shows reduced areas and less well defined preferred orientation patterns.

These results show that the variations of preferred orientation patterns in the less competent matrix are critically dependent on the fold geometries in the competent layers. Since the differences of the competency

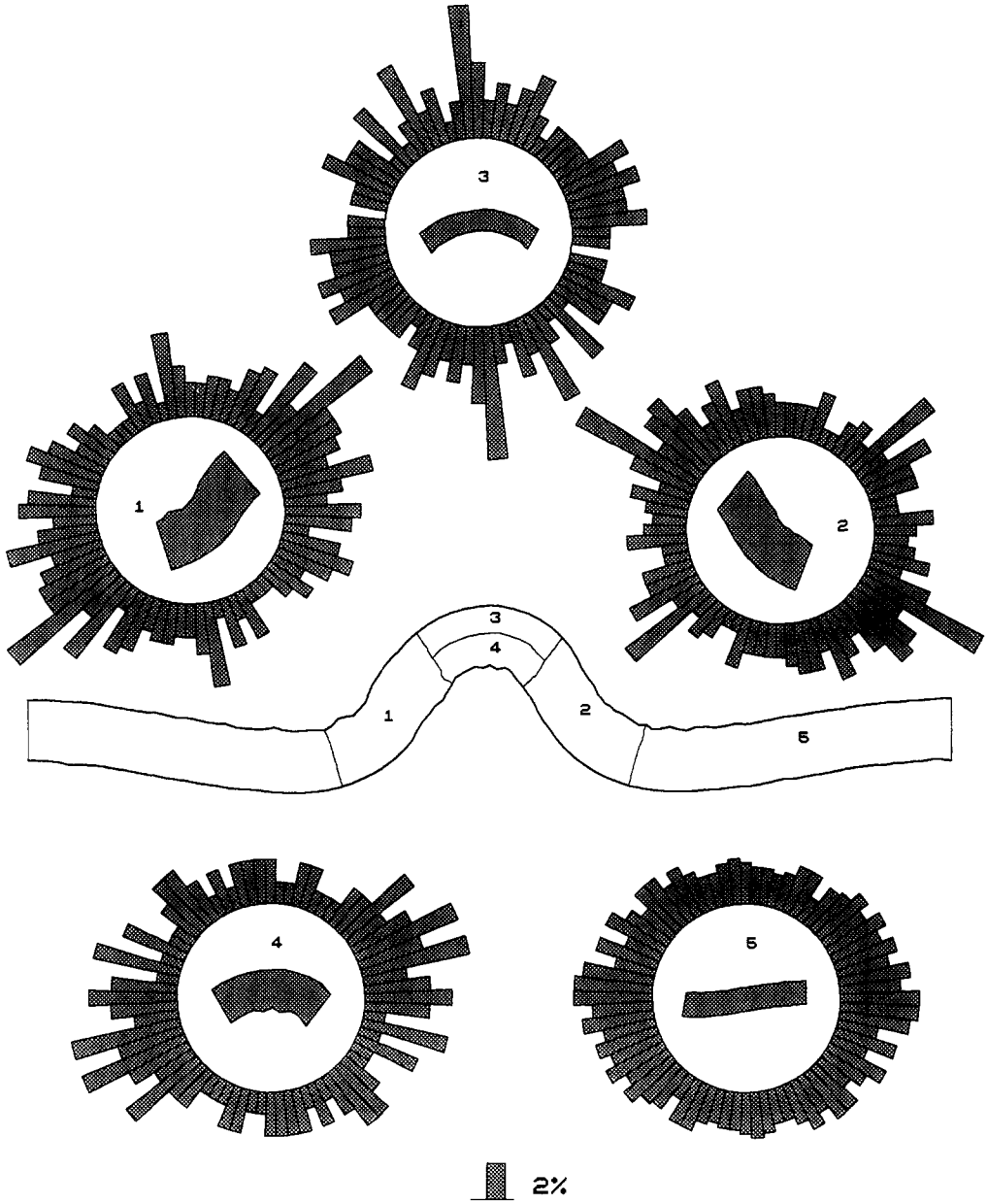

Fig. 5. The sub-area divisions of the competent layer and the orientation distributions of slip-plane normals for these sub-areas (the model with $R = 5$).

contrasts between the two models has effectively led to the formation of folds with different geometries (mainly amplitude) (see Fig. 3), the fabric results of the two models for the matrix must show some differences. In general, the fabric development for the high competency contrast model is stronger.

The fabric results for the less competent matrix could be relevant to cleavage development in the soft stratum rocks next to a folded high-competency bed. These experiments support the idea that cleavages do not develop always parallel to the fold axial plane. Different orientation relationships between cleavage and the fold axial plane exist in the different positions of the less competent rocks with respect to the folded layer. In particular, the current results show that the cleavage developed in the less competent rocks in the vicinity of the outer arc of a fold hinge zone could be normal to the fold axial plane (see Fig. 8).

DISCUSSION

The results of this computer model indicate that the development of crystallographic preferred orientations is much weaker in the competent layer than in the less competent matrix, and changing the competency contrast in the model has an influence on the fabric outcome. These can be understood by examining the mechanical and deformational response of the numerical specimen assembly during buckling.

The assembly in the present model is a stiff thin layer embedded in the thick soft matrix with a striking competency contrast. In the process of deformation, the competent layer and the less competent matrix behave differently. The central thin stiff layer, which has a higher yield limit (higher τ_c on slip planes), can sustain higher stresses than the soft matrix before the limit is reached. In so doing, the layer acts as a stress supporting

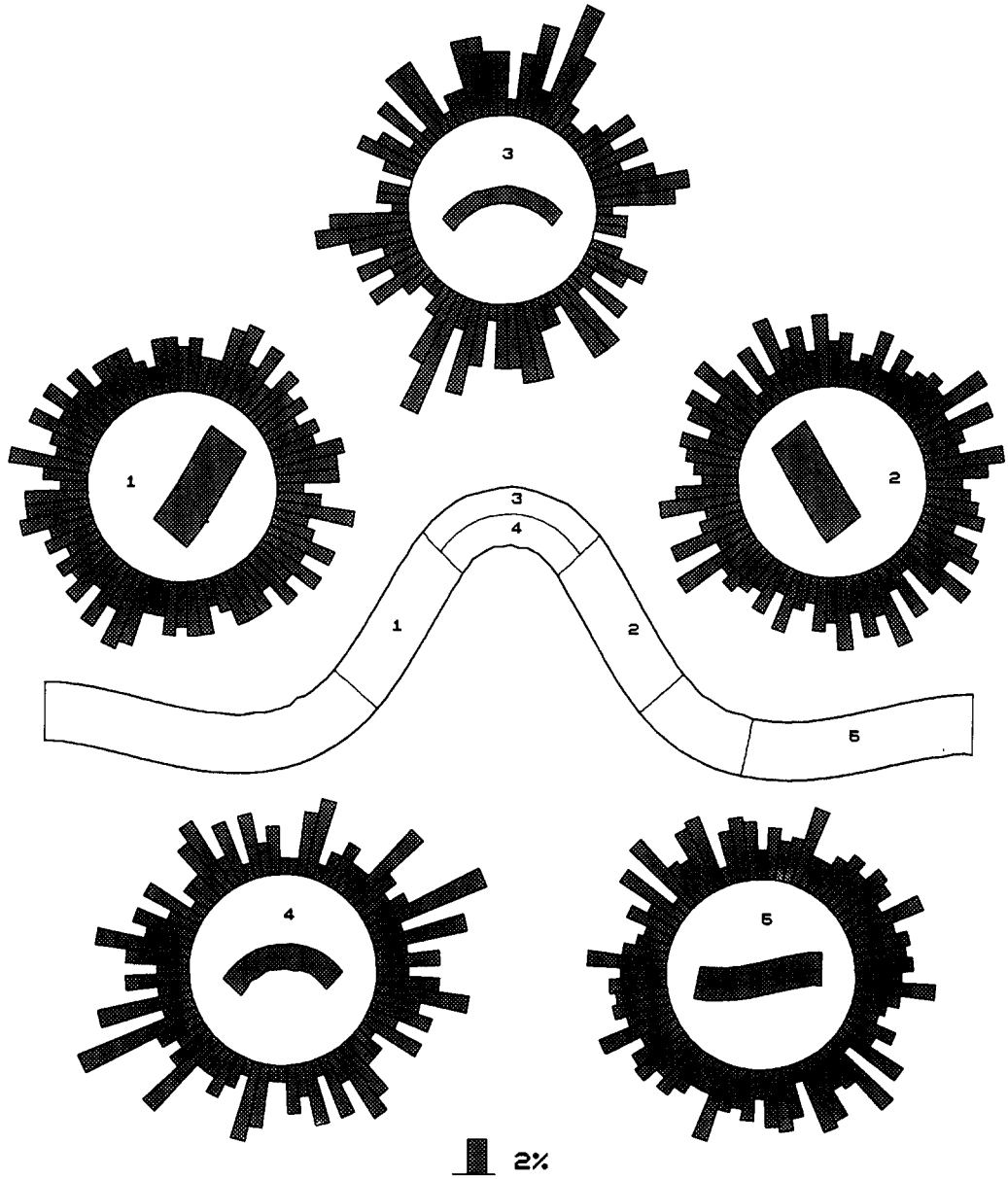

Fig. 6. The sub-area divisions of the competent layer and the orientation distributions of slip-plane normals for these sub-areas (the model with $R = 100$). In contrast to Fig. 5, an area between areas 2 and 5 is excluded here because this area differs from the limb and unbuckled-layer parts but resembles a hinge zone; the inclusion of this area would cause the weakening of the preferred orientation of the resulting fabrics.

beam, and buckling which does not contribute much to the intra-layer strain is the major response of the layer to the imposed bulk shortening, even though a small amount of pre-buckling layer-parallel shortening also occurs. Therefore, as shown in Fig. 9, the buckled competent layers are characterized by high stresses and low strains. Low strains are obviously disadvantageous to fabric development. It is known that competency contrast is the parameter determining the partitioning of bulk shortening between the buckling and the pre-buckling layer-parallel shortening. A higher competency contrast means a higher yielding contrast which gives rise to larger buckling and smaller pre-buckling shortening (smaller intra-layer strain), and vice versa. Owing to this, the strain in the competent layer and the stress contrast between the layer and the matrix for the model of $R = 5$ are, respectively, larger and smaller than those for the model of $R = 100$ (Fig. 9). This explains why the competent layer in the model of $R = 5$ exhibits distinguishable fabric patterns while the layer in the model with $R = 100$ shows poor fabric development. In contrast to the situation of the competent layers, the less competent matrices with a low yield limit experience an early plastic yielding while stresses are still low, and thereafter they cannot resist any further external loading since any attempt for stresses to increases will be relaxed by simultaneous plastic flow. Therefore, extensive plastic shortening is the major response to the imposed bulk shortening, and the matrix characteristically exhibits low stresses but high strains (Fig. 9). As a result, fabrics are well developed.

Two episodes of fabric development in the single-layer buckling system could be recognized from the current results, that is, layer-parallel bulk shortening and buckling. In different sub-areas of the system, each or both could be important. In the competent layer, the

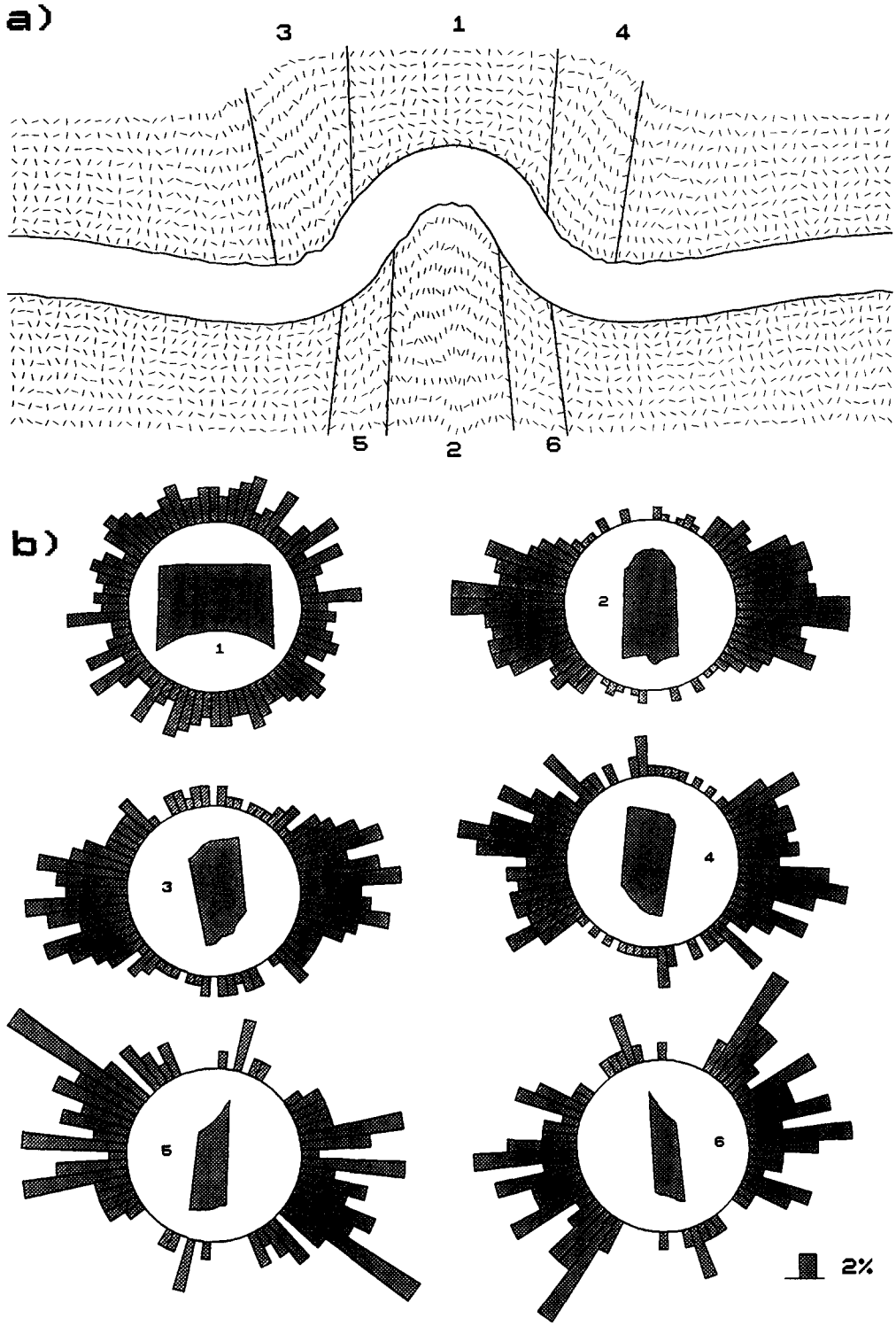

Fig. 7. The fabric results for the less competent matrix in the model of $R = 5$. (a) The final slip-plane traces in the deformed matrix and the sub-area divisions of the matrix. (b) The preferred orientations of slip-plane normals for six sub-areas.

preferred orientation of slip-plane normals for the unbuckled-layer area (see 5 in Fig. 5) is obviously due to the bulk shortening, those for the limb areas (see 1 and 2 in Fig. 5) seem to be produced by the bulk shortening and then subjected to a buckling rotation, and those for the hinge zone areas (see 3 and 4 in Fig. 5) result dominantly from the buckling-induced secondary extension and shortening. In the less competent matrix, the preferred orientations are always the results of mutual operation of the two episodes of deformation since the shortening of the matrix must accommodate the buckling of the competent layer. This explains why the fabric patterns in the matrix vary from area to area along the buckled competent layer, and why the fabrics in the matrix of the model ($R = 100$) involving a larger buckle are better developed than in the matrix of the model ($R = 5$) involving a smaller buckle. An area of interest is the one near the outer arc of the hinge zone (see 1 in Figs. 7 and 8), where the effects of the bulk shortening and the buckling-induced extension are approximately

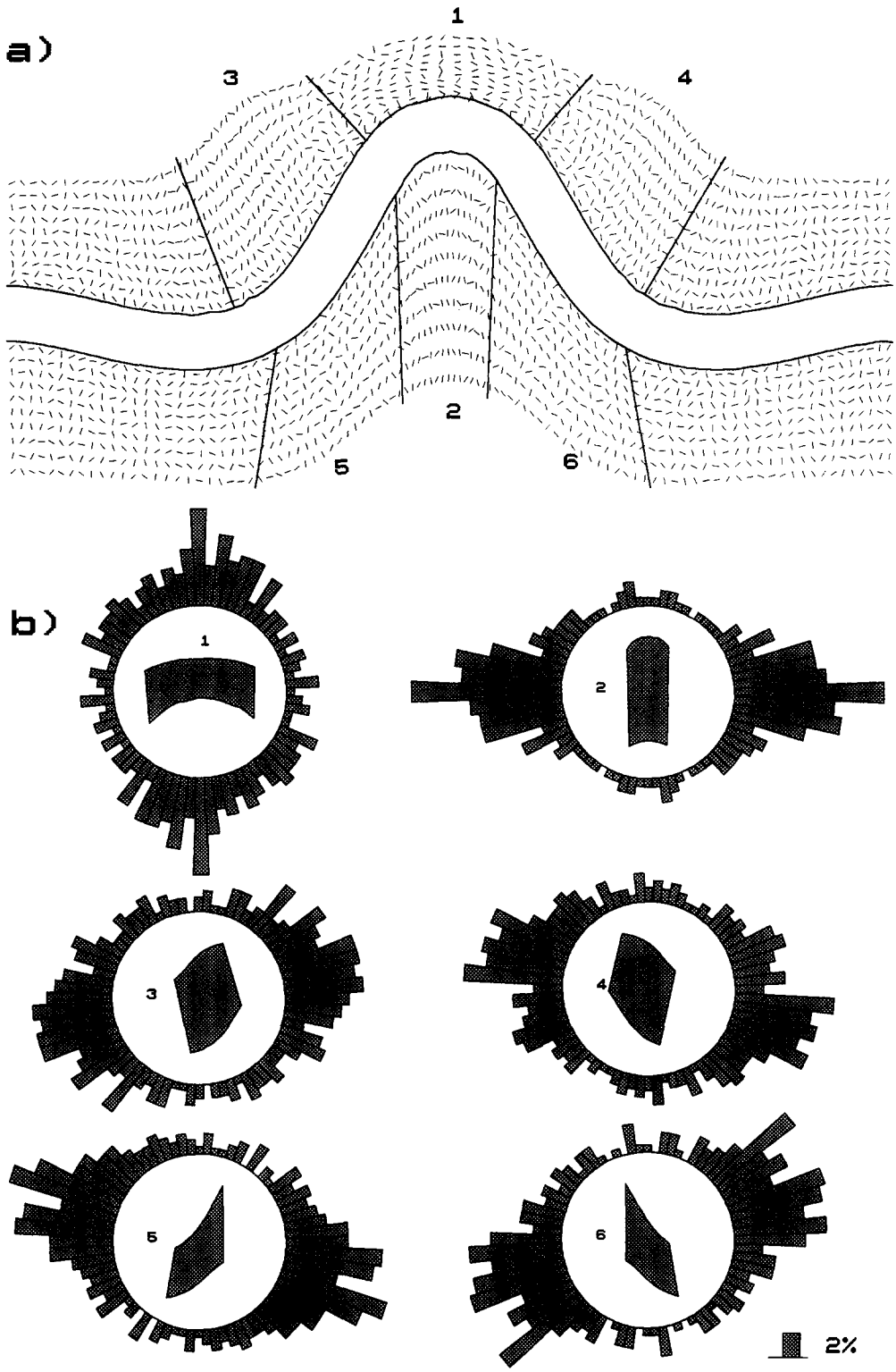

Fig. 8. The fabric results for the less competent matrix in the model of $R = 100$. (a) The final slip-plane traces in the deformed matrix and the sub-area divisions of the matrix. (b) The preferred orientations of slip-plane normals for six sub-areas.

opposite. When the buckling is so strong that the extension overwhelms the effect of bulk shortening, as in the model of $R = 100$, buckling fabrics are developed. If the extension is just enough to cancel the effect of bulk shortening, as in the model of $R = 5$, the fabric development then is poor. With this in mind, the preferred orientations of slip-plane normals, developed in this area, could be used as an indicator of the strength of pre-buckling layer-parallel shortening in situations where folds are well grown. The development of a preferred orientation parallel to the fold axial plane should indicate a small amount of pre-buckling layer-parallel shortening, the effects of which have been totally eliminated by the buckling-induced extension, whilst the development of a preferred orientation normal to the fold axial plane (or a poor fabric pattern) should be an indication

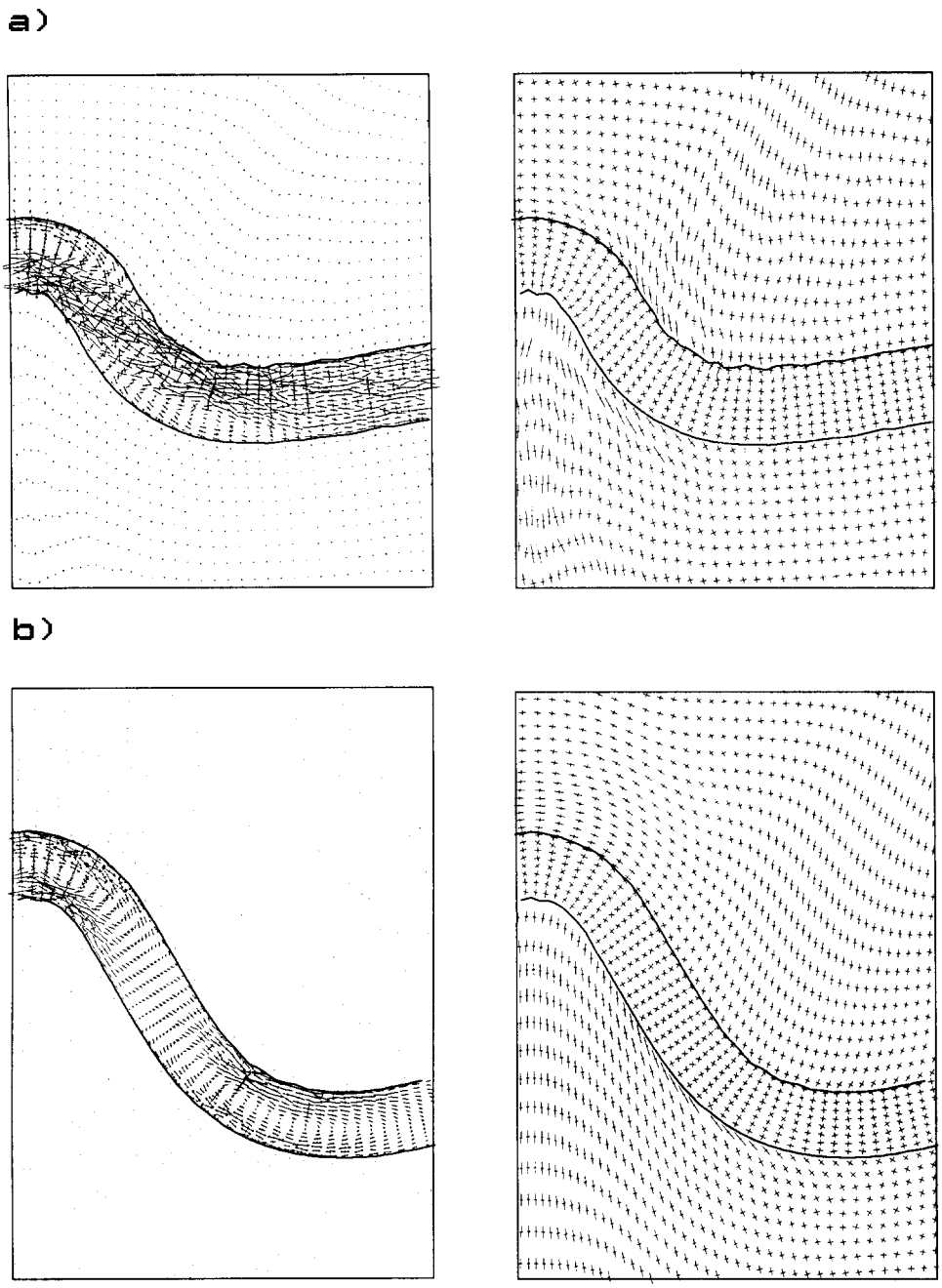

Fig. 9. The orientation and magnitude of principal stresses (left) and strains (right) in the chosen parts of the deformed specimens. (a) The model of $R = 5$; (b) the model of $R = 100$. In the stress plot, the length of the bars is proportional to stress magnitude, and the bars with arrow heads indicate tensile stresses.

of a relatively large amount of shortening. In contrast to the outer-arc sub-area, in the area adjoining the inner arc of the hinge zone (see 2 in Figs. 7 and 8), the effects of bulk shortening and the buckling-induced shortening are positively superimposed and strong preferred orientations normal to the fold axial plane are always developed.

There have been many reports that strong crystallographic preferred orientation patterns are observed in investigations of natural folds (e.g. Carreras *et al.* 1977, Dietrich 1986). Gairola (1989) also showed that clear preferred orientations occurred in the hinge zones of his experimentally produced folds in marble and limestone. In contrast to these natural and experimental results, the fabric development in the competent layers of the present model appears to be relatively weak, particularly in the layer of the high competency contrast model ($R = 100$), where intra-layer strain is very small. This difference can in part be explained, since natural folds generally involve geological sequences in which the competency contrasts between the neighbouring beds can be quite small. At the same time, folded rocks usually experience strong deformation and show high strains (e.g. Mitra 1978), so well developed fabrics are to be expected. High strain is also possibly involved in Gairola's experimentally formed folds since the experiment involves the folding of marble and limestone plates (without a soft matrix) under conditions of relatively high temperature (400°C) and low strain rate ($\times 10^{-7}$ s^{-1}). These deformational conditions could also give

rise to a certain degree of dynamic recrystallization and twinning in calcite, which are both factors favourable for fabric development.

It is noted that, although various preferred orientations are developed for various sub-areas in the deformed numerical specimens, the preferred orientations of the slip-plane normals are all approximately parallel to the local principal shortening directions. This is basically consistent with previous simulation results of fabric development in polycrystalline aggregates containing one slip system (Etchecopar 1977, Zhang *et al.* 1991), and with the crystallographic preferred orientation developed in experimentally flattened synthetic dunites (Nicolas *et al.* 1973).

In this model, some small secondary perturbations have been generated along the boundary surface between the competent layer and the matrix in the inner arc of the hinge zone (see Fig. 3). These are the geometrical manifestations of mesh deformation under the condition where strong buckling-induced local shortening operates, and where strong interaction between the layer and the matrix exists. This could possibly be overcome by using a finer mesh. It should also be mentioned that the uniform distributions of slip-plane orientations, as shown in Fig. 2, are ensured only precisely for the whole competent layer and the whole matrix. The distribution for a local sub-area could show slight deviation from these patterns. This is why the fabrics for some sub-areas in the hinge zones of the buckled competent layers, where deformations are too weak, are not precisely symmetrical about the fold axial plane (see 4 in Fig. 5; 3 and 4 in Fig. 6).

CONCLUSIONS

(1) The numerical simulation of fabric development in the single-layer buckling assembly shows that the preferred orientation of slip planes is generally well developed in the less competent matrix but poorly developed in the buckled competent layer.

(2) The competency contrast in a model has an influence on the fabric development. For competent layers, the high contrast model produced no preferred orientation, whereas the low contrast model still showed distinguishable preferred orientations. For the less competent matrix, in contrast, the high contrast model offered better fabric development than the low contrast model.

(3) Distinct preferred orientations of slip-plane normals are developed for the different sub-areas of the assembly. These preferred orientations have different orientation relationships to the fold axial plane, ranging from parallel to normal. In general, the slip planes are preferentially oriented approximately parallel to local principal extension (elongation) directions.

(4) With progressive bulk shortening the fabric orientation is transposed in the outer arc sub-areas where buckling-induced horizontal extension is superimposed on layer-parallel shortening.

Acknowledgement—The authors would like to thank W. D. Means for his useful comments and suggestions on the work during his visit to CSIRO Division of Geomechanics.

REFERENCES

Abbassi, M. R. & Mancktelow, N. S. 1990. The effect of initial perturbation shape and symmetry on fold development. *J. Struct. Geol.* **12**, 273–282.

Biot, M. A. 1957. Folding instability of a layered viscoelastic medium under compression. *Proc. R. Soc. Lond.* **A242**, 444–454.

Biot, M. A. 1959a. Folding of a layered viscoelastic medium derived from an exact stability theory of a continuum under initial stress. *Qt. Appl. Math.* **17**, 185–204.

Biot, M. A. 1959b. On the instability of folding deformation of a layered viscoelastic medium in compression. *J. Appl. Mech.* **26**, 393–400.

Biot, M. A. 1961. Theory of folding of stratified viscoelastic media and its implications in tectonics and orogenesis. *Bull. geol. Soc. Am.* **72**, 1595–1620.

Board, M. 1989. FLAC: Fast Lagrangian Analysis of Continua, Version 2.20, Software Summary. Itasca Consulting Group, Inc., Minneapolis.

Carreras, J., Estrada, A. & White, S. 1977. The effects of folding on the *c*-axis fabrics of a quartz mylonite. *Tectonophysics* **39**, 3–24.

Chapple, W. M. 1968. A mathematical theory of finite amplitude rock folding. *Bull. geol. Soc. Am.* **79**, 47–68.

Clark, S. P., Jr (editor) 1966. *Handbook of Physical Constants. Mem. geol. Soc. Am.* **97**.

Cobbold, P. R. 1975. Fold propagation in single embedded layers. *Tectonophysics* **27**, 333–351.

Cobbold, P. R. 1977. A finite-element analysis of fold propagation—a problematic application. *Tectonophysics* **38**, 339–353.

Cundall, P. A. 1989. Numerical experiments on localization in frictional materials. *Ing. Arch.* **59**, 148–159.

Cundall, P. A. 1990. Numerical modelling of jointed and faulted rock. In: *Proc. Int. Conf. on Mechanics of Jointed and Faulted Rock*, 11–18.

Cundall, P. A. & Board, M. 1988. A microcomputer program for modelling large-strain plasticity problem. In: *Numerical Methods in Geomechanics* (edited by Swobada, C.). Balkema, Rotterdam, 2101–2108.

Dietrich, D. 1986. Calcite fabrics around folds as indicators of deformation history. *J. Struct. Geol.* **8**, 655–668.

Etchecopar, A. 1977. A plane kinematic model of progressive deformation in a polycrystalline aggregate. *Tectonophysics* **39**, 121–139.

Gairola, V. K. 1989. Calcite fabrics in the hinge zones of experimentally folded single layers of marble and limestone. *J. Struct. Geol.* **11**, 343–347.

Hobbs, B. E. & Ord, A. 1989. Numerical simulation of shear band formation in a frictional-dilational material. *Ing. Arch.* **59**, 209–220.

Hobbs, B. E., Mühlhaus, H.-B. & Ord, A. 1990. Instability, softening and localization of deformation. In: *Deformation Mechanisms, Rheology and Tectonics* (edited by Knipe, R. J. & Rutter, E. H.). *Spec. Publs geol. Soc. Lond.* **54**, 143–165.

Hudleston, P. J. 1973a. An analysis of "single-layer" folds developed experimentally in viscous media. *Tectonophysics* **16**, 189–214.

Hudleston, P. J. 1973b. Fold morphology and some geometrical implications of theories of fold development. *Tectonophysics* **16**, 1–46.

Itasca Consulting Group 1991. FLAC: Fast Lagrangian Analysis of Continua, User Manual, Version 3.0. Itasca Consulting Group, Inc., Minneapolis.

Lister, G. S., Paterson, M. S. & Hobbs, B. E. 1978. The simulation of fabric development in plastic deformation and its application to quartzite: the model. *Tectonophysics* **45**, 107–158.

Mitra, S. 1978. Microscopic deformation mechanisms and flow laws in quartzites within the South Mountain anticline. *J. Geol.* **86**, 129–152.

Nakaya, U. 1954. The deformation of single crystals of ice. *J. Glaciol.* **2**, 229–240.

Nicolas, A., Boudier, F. & Boullier, A. M. 1973. Mechanisms of flow in naturally and experimentally deformed peridotites. *Am. J. Sci.* **273**, 853–876.

Nicolas, A. & Poirier, J. P. 1976. *Crystalline Plasticity and Solid State Flow in Metamorphic Rocks*. Wiley, New York.

Ord, A. 1990. Mechanical controls on dilatant shear zones. In:

Deformation Mechanisms, Rheology and Tectonics (edited by Knipe, R. J. & Rutter, E. H.). *Spec. Publs geol. Soc. Lond.* **54**, 183–192.

Ramberg, H. 1959. Evolution of ptygmatic folding. *Norsk geol. Tiddskr.* **39**, 99–151.

Ramberg, H. 1960. Relationship between length of arc and thickness of ptygmatically folded veins. *Am. J. Sci.* **258**, 36–46.

Ramberg, H. 1961. Contact strain and folding instability of a multilayered body under compression. *Geol. Rdsch.* **51**, 405–439.

Ramsay, J. G. 1967. *Folding and Fracturing of Rocks*. McGraw-Hill, New York.

Sherwin, J. A. & Chapple, W. M. 1968. Wavelengths of single layer folds: a comparison between theory and observation. *Am. J. Sci.* **266**, 167–179.

Williams, J. R., Lewis, R. W. & Zienkiewicz, O. C. 1978. A finite-element analysis of the role of initial perturbations in the folding of a single viscous layer. *Tectonophysics* **45**, 187–200.

Zhang, Y., Hobbs, B. E. & Ord, A. 1991. Preferred orientation development of polycrystals with one slip system and with grain boundary sliding (extended abstract). In: *Cratonic Margins: Structural and Tectonic Process, The 6th SGTSG Conference*. Geological Society of Australia, 85–86.